OPEN ACCESS

# ACTA METALLURGICA SLOVACA

2020, VOL. 26, NO. 3, 126-131

**RESEARCH PAPER**

## CORROSION AND WEAR PERFORMANCE OF ZA27/GRAPHENE/$B_4C$ HYBRID NANOCOMPOSITES PRODUCED BY POWDER METALLURGY

Emre Deniz Yalçin[1], Aykut Çanakçi[2]

[1] Karadeniz Technical University, Abdullah Kanca Vocational High School, Trabzon, 61530, Turkey, emredenizyalcin@ktu.edu.tr

[2] Karadeniz Technical University, Department of Metallurgical and Materials Engineering, Trabzon, 61080, Turkey, aykut@ktu.edu.tr

*Corresponding author: emredenizyalcin@ktu.edu.tr tel.: 0462 377 81 70, Karadeniz Technical University, Abdullah Kanca Vocational High School, Trabzon, 61530, Turkey

Received: 27.04.2020
Accepted: 11.08.2020

**ABSTRACT**

In this research paper, dry sliding (unlubricated), corrosion and abrasive wear behavior of ZA27/ Graphene/ $B_4C$ hybrid nanocomposites were studied. The hybrid nanocomposite samples were fabricated by powder metallurgy technique. Tribological tests were performed by employing a ball-on-disc type in the unlubricated situation and different loads (1, 2, 5 and 10 N). The examination of the worn and corroded surfaces, the powder characterization was performed using scanning electron microscopy (SEM). The findings indicated that the increase in $B_4C$ nano-particle content can positively effect on the corrosion and wear behavior of the hybrid nanocomposites. The electrochemical polarization measurements showed that increasing of the nano $B_4C$ content causes high corrosion resistance in the hybrid nanocomposites. The corrosion tests showed that the corrosion rate value of the ZA27/Graphene/$B_4C$ hybrid nanocomposites decreased from 59.02 mpy to 16.77 mpy with increasing the nano $B_4C$ content from 0.25% to 2%.

**Keywords:** ZA27, Graphene, $B_4C$, Hybrid nanocomposite, Wear, Corrosion

### INTRODUCTION

Reinforcement of ZA27 alloys, with different materials, improve the strength of these alloys through better mechanical and physical properties. As a result, in recent years, Zn-Al based metal matrix composites (MMCs) have been used as alloys with lighter weight and high wear resistance [1-4]. In recent studies, $B_4C$ ceramic particles are used to improve mechanical strength and increase thermal stability. The most important reason for using $B_4C$ particles instead of SiC and $Al_2O_3$ ceramic particles is that $B_4C$ particles have a relatively low density compared to SiC and $Al_2O_3$ particles and therefore the nanocomposites to be produced using $B_4C$ particles have a higher specific strength value [5].

In recent years, graphene has emerged as a promising reinforcement material to advance wear resistance in hybrid nanocomposite materials. In this regard, many researches have been reported in the area of hybrid nanocomposites where the addition of graphene as a second phase leads to the development of the tribological and mechanical properties [6,10].

Graphene, as a very rigid material with low friction, is a perfect choice of material for bearing applications and nano-sized objects, including friction reduction and wear protection [7]. Mitrović et al. [8] have studied the wear behaviors of ZA27/Graphite/SiC hybrid nanocomposites manufactured by compo-casting. Their study showed that the ZA27/SiC/Graphite hybrid nanocomposites had greater wear resistance than ZA27 for all the sliding speeds and loads. In a recent study, the abrasion and corrosion behavior of nanocomposites produced by using in the range of 0.125 wt %-3 wt % nanographene reinforcement in ZA27 matrix alloy was investigated. According to the results, the hardness values of the samples decreased with increasing nanographene supplementation while increasing the abrasion resistance. In particular, 3 wt% nanographene reinforcement significantly improved the wear and corrosion properties. The corrosion rate for ZA27 was 2.719 mpy and the ZA27-Graphene nanocomposite supplemented with 3 wt% nano-graphene was 1.745 mpy [9]. Girish et al. [10] studied the wear behavior in the dry sliding environment by reinforcing the ZA27 matrix with graphite for tribological applications. In that study, 0%, 4%, 6%, 8% by weight graphite was added to the ZA27 matrix and it was found that the resistance to abrasion was best achieved with 4 wt % to 6 wt % graphite reinforcement.

The previous reports showed that nanoparticles reinforced with hybrid nanocomposites exhibit good tribological and mechanical properties. Because the unwished phases between the alloy and nanoparticles are inhibited at low increase the hardness of composite to uniformly dispersive in the matrix [11]. Dalmıs et al. investigated the mechanical and physical properties of ZA27-$B_4C$. Their experimental data indicated that nano $B_4C$ can be used to enhance the mechanical and physical properties of the ZA27 matrix alloy. The increase in nano-sized $B_4C$ ratio can cause the formation of agglomeration in grain size boundaries, which explains the decrease in tensile strength, density, and hardness values [12]. Dou et al. studied the wear behavior of Al6061 alloy matrix composites reinforced with 20% $B_4C$ ceramic particles and stated that the wear loss was high at the beginning of the wear process and this loss was decreased as the wear rate increased and the oxide formation had a significant effect on the wear behavior [13]. In a study by Rajkumar and Aravindan, 5% to 30% by weight of graphite-reinforced and copper-based composite materials used in bearing materials were produced and density and hardness values of the produced materials were investigated. According to the results of this study, increasing the graphite amount and density caused a decrease in hardness values. The sintered density values decreased from approximately 7.6 g/cm$^3$ to 6.6 g/cm$^3$ and the hardness value decreased from 85 Hv to 55 Hv. The reason for the decrease in density values was attributed to the increasing amount of graphite and the increase in the number of aggregation regions formed by graphite particles in the structure and the decrease in hardness to the low hardness of graphite [14]. Seah et al. examined the acidic corrosion values of the composites they produced by adding 0%, 1%, 3%, 5% of graphite in the Zn-Al alloy matrix. Corrosion tests were performed at room temperature for 12 to 60 hours. They found that the wear decreases in HCl solution, while it increases with the addition of graphite [15]. Bobic et al. investigated the corrosion behavior of composites produced by the casting method by adding 1-3-5% $SiC_P$ particles to ZA27 alloy. In the corrosion tests, 3.5% NaCl-(pH 6.7) was used as the test solution. After electrochemical polarization measurements, it was seen that increased $SiC_P$ rate decreased the corrosion resistance of composites [16]. Morphology has a significant effect on the corrosion properties of metallic materials and alloys used in the industry. However, the physical and mechanical resistance of materials and alloys determine the amount of homogeneity in the distribution of the second phase [17-19].

Recent studies, showed that the form and content of the reinforcement material in the ZA27 matrix, the production technique of reinforced ZA27 and its hybrid nanocomposites play a very important function on the wear properties of nanocomposites. Nevertheless, to the author's knowledge, the effect of the reinforcement content on the corrosion and wear behavior of ZA27-based nanocomposites reinforced with nano-size graphene and nano-size $B_4C$ has not been studied using powder metallurgy method. It should be also noted that

previous researches were just focused on the use of different reinforcement materials into the ZA27-based matrix. However, in this research, the effect of ZA27-based hybrid nanocomposites on the distribution of the nanoparticles in the ZA27 alloy was also studied. Hence, the aim of this research is graphene and $B_4C$ reinforced zinc-aluminum based ZA27 matrix and hybrid nanocomposite materials; production by combining with powder metallurgy and mechanical alloying techniques, which have an important place in the production of materials. Also, the physical, morphological, and mechanical (hardness, abrasion resistance, and corrosion resistance) properties of the new materials produced were investigated.

## MATERIAL AND METHODS

In this research paper, ZA27 powders (İki El Metal Co.) with average particle size 40 nm and a theoretical density of 5 g/cm$^3$ were used as the matrix alloy. $B_4C$ and graphene powders (Alfa Aesar) with an average particle size of 50 nm and 55 nm were employed as reinforcement materials. The nominal composition of the ZA27 alloy listed in Table 1 [20,21]. Table 2 shows the coded of hybrid nanocomposites and their reinforcement content. ZA27 matrix alloy and its hybrid nanocomposites with different content of $B_4C$ nanoparticles (0.25, 0.5, 1 and 2 wt. %) and graphene nanoparticles (3 wt. %) were produced by mechanical milling. Retsch PM 100 planetary ball-mill (high energy ball milling) is used in the milling process of hybrid nanocomposites. Powder mixing was carried out for 1 hour at room temperature in an argon atmosphere. The milling process was made of a tungsten carbide mill chamber with a volume of 250 ml, balls of 10 mm diameter. The ball: powder weight ratio was selected as 5:1. Mechanical mixing was carried out at Argon atmosphere, at room temperature and at a grinding speed of 400 rpm. The addition of zinc-stread was made at a rate of wt. 1% to prevent agglomeration during mechanical milling. Hot pressing was used for the preparation of the ZA27 matrix alloy and its hybrid nanocomposites. ZA27 matrix alloy and its hybrid nanocomposites powder were manually put consecutively in the steel die, and then the powders were uniaxial cold-pressed in a die up to 200 MPa for 2 minutes. The green compacts of ZA27 based hybrid nanocomposites in the die were hot-pressed for 3 hours at 435 ºC and 500 MPa in an argon atmosphere. The density of the sintered samples was determined by the Archimedes method. Morphology and internal structure analysis of hybrid nanocomposite powders were investigated by using a ZEISS LS 10 scanning electron microscope (SEM). Distribution of reinforcements in the matrix, porosity and surface investigations were made in detail by SEM analysis. After the wear and corrosion tests in SEM, the type of wear and surface condition and corrosion damage on the surface were examined. Rigaku Corporation, Japan brand X-ray diffractometer (XRD) was used for phase identification of ZA27/Graphene/$B_4C$ hybrid nanocomposite samples. This was carried out at 40kV and 30mA and under Cukα (1,54059 Ao) radiation. XRD patterns were performed between 10-80 ° and 2θ.

Wear behavior of the ZA27 and its hybrid nanocomposites were examined by using a ball on disc (DUCOM) tribology tester. The tests were performed in dry sliding and 60 % relative humidity at room temperature. On account of wear test, ZA27 and its hybrid nanocomposite samples were ground with a 1500-2000 SiC grinding paper and further cleaned in ethanol. Before wear tests, the initial weights of the samples were measured. Balls made of H11 hot work tool steel with a diameter of 10 mm were used as abrasives. Before the wear tests, the surface roughness (Ra) values of the samples were measured as 0.2 µm. Wear test specimens were produced with a diameter of 30 mm and two different loads were used on one surface and a total of four loads were used on both surfaces. The applied loads were 1, 2, 5 and 10 N at 100 rpm (sliding speed range) and the sliding distances were chosen as 300 m. GAMRY reference 3000 brand corrosion device was used in corrosion tests. Corrosion samples were first drilled to a diameter of 2 mm. A copper wire was contacted with the sample to provide the electron current. The samples were ground with 600, 800, 1200 and 1500 grit and polished with alumina. The surface of each sample was washed with methanol and dried before starting the corrosion tests Potentiodynamic polarization tests were performed to determine the corrosion resistance of ZA27 / Graphene / $B_4C$ hybrid nanocomposite samples. Potentiodynamic polarization measurements were started with a cathodic potential of 500 mV and continued to the anodic potential of + 500 mV at a scanning rate of 1 mV/s. In the experiments, a 3.5% NaCl solution was used as the electrolyte. To determine the corrosion resistance of ZA27 matrix alloy and hybrid nanocomposite samples, two potentiodynamic polarization tests were performed and averaged.

**Table 1** Chemical composition of ZA27 alloy (wt.%)

| **Al** | **Cu** | **Mg** | **Zn** |
|---|---|---|---|
| **25,8** | 2,4 | 0,012 | Bal. |

**Table 2** The samples produced by mechanical alloying and then hot pressing

| Sample Number | Milling Time (h) | ZA27 (wt. %) | Graphene (wt. %) | B4C (wt. %) |
|---|---|---|---|---|
| ZA27 | 1 | 100 | 0 | 0 |
| ZGB-0.25 | 1 | 96.75 | 3 | 0.25 |
| ZGB-0.5 | 1 | 96.5 | 3 | 0.5 |
| ZGB-1 | 1 | 96 | 3 | 1 |
| ZGB-2 | 1 | 95 | 3 | 2 |

## RESULTS AND DISCUSSION

### Subtitle of results and discussion

In this study, nanocomposite and hybrid nanocomposites were produced by using the powder metallurgy method by reinforcing ZA27 matrix material with nano-size graphene and $B_4C$. The effects of nano-size graphene and $B_4C$ on hardness, microstructure, wear and corrosion behavior of the ZA27/Graphene/$B_4C$ hybrid nanocomposite were investigated. The main results obtained from experimental studies are discussed below.

### XRD Analyses

XRD patterns of ZA27 matrix alloy and ZA27/Graphene/$B_4C$ hybrid nanocomposites which have different graphene nanoparticle contents are presented in Fig. 1. The peaks of Zn, Al, and $CuZn_5$, besides that graphene, can be seen in the XRD pattern. When compared with the ZA27 matrix, newly produced phases such as the graphene phase were observed for ZA27/Graphene/$B_4C$ hybrid nanocomposites, while the diffraction peaks of $B_4C$ phase were much low for ZGB-0.5 hybrid nanocomposite. The increase in diffraction peak intensity of $B_4C$ was observed for the ZGB-2 hybrid nanocomposite (Fig. 1). As shown in Fig. 1, the amount of $CuZn_5$ intermetallic phases increased for the hybrid composites. It should be noted that the $CuZn_5$ phase can be formed in the Zn–Al–Cu phase diagrams at a reaction temperature of 450 °C [22-23]. This result can be attributed to the positive effect of graphene on the formation of intermetallic phases and the densification process. As known, carbon-based materials such as graphite, graphene, and carbon nanotube have high thermal conductivity and the high conductivity of graphene particles increases the diffusion ability between Cu and Zn elements during the hot pressing process. Therefore, $CuZn_5$ phase content increases with increasing graphene content. A Similar result has been observed in a previous study [24].

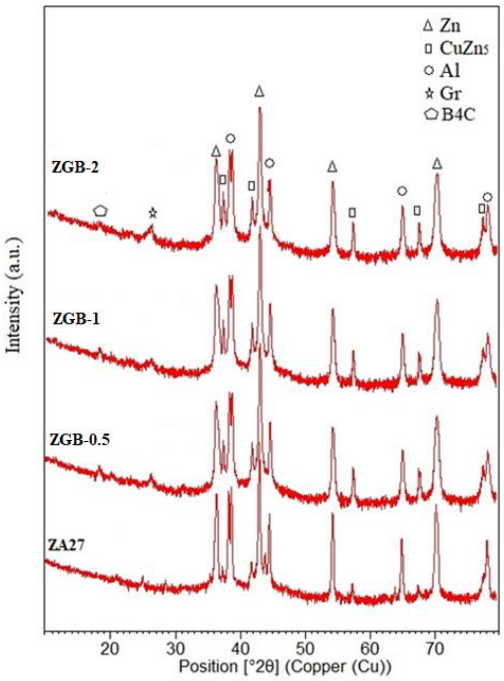


**Fig. 1** XRD patterns of ZA27 alloy and ZA27/Gr/$B_4C$ hybrid nanocomposite for different $B_4C$ content

**Microstructure**

The SEM images of $B_4C$, graphene, and ZA27 matrix alloy powders are given in Fig. 2. ZA27 matrix powders were in ligament and irregular structure while $B_4C$ powders were in a polygonal and angular structure. Graphene powders were hexagonal structure. (Fig. 2. and Fig. 3). Fig 3 also shows the morphology of hybrid nanocomposite powders with different reinforcement content after milling time of 1h. After 1 hour of milling, $B_4C$ was embedded into the ZA27 powders surrounded with nano-size graphene particles The nearly flaked morphology of particles proposes that the 1 h milling time was enough to reach the desired condition.

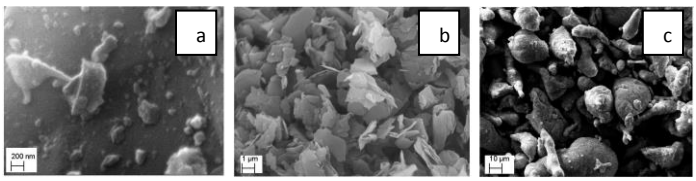


**Fig. 2** SEM images of the initial matrix powders and reinforcement particles, (a) nano $B_4C$ particles, (b) nano graphene particles, (c) ZA27 alloy powders.

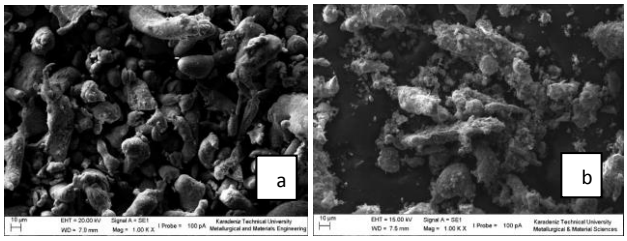


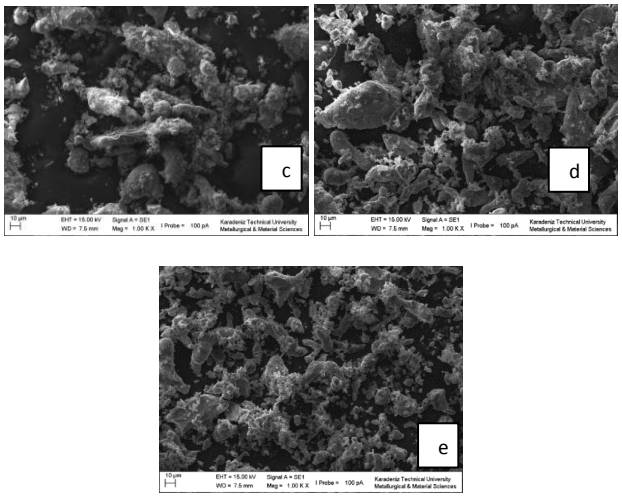


**Fig. 3** SEM images of ;a) ZA27, b) ZGB-0.25 hybrid nanocomposite powders, c) ZGB-0.5 hybrid nanocomposite powders, d) ZGB-1 hybrid nanocomposite powders and e) ZGB-2 hybrid nanocomposite powders ball milled for 1h

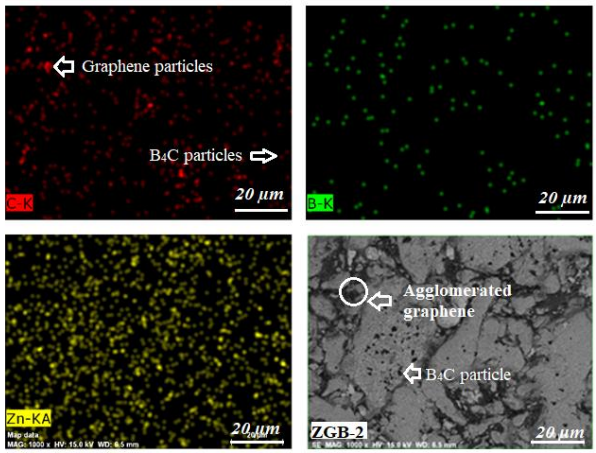


**Fig. 4** SEM mapping images of ZGB-2 hybrid nanocomposite.

Fig. 4 shows SEM-EDS element distributions belonging to ZGB-2 hybrid nanocomposites. According to these internal structures, the red, green, blue, and yellow regions indicate the elemental distribution of C, B, Al, and Zn, respectively. Red regions show the distribution of nano-size graphene particles, while the green points indicate the nano $B_4C$ particles into the ZA27 alloy matrix. The mapping confirmed that the distribution of nanoparticles in the matrix was nearly homogenous. As can be seen in the C-K mapping that showing with red point, agglomerated graphene particles are only located within the boundaries between neighboring ZA27 alloy matrix particles. While the $B_4C$ particles are embedded in the matrix particles.

**Porosity and Harness Measurements**

The density decreased with increasing reinforcement. ZA27/Graphene/$B_4C$ sample has a lower density than ZA27 due to its lower densification ability and the more agglomeration. The porosity of hybrid nanocomposites increased with the increase in the $B_4C$ content. This can be attributed to the effect of hot pressing during the densification. The increase in the $B_4C$ content from 1wt% to 2 wt% resulted in a decrease in the density of hybrid nanocomposites, nevertheless an important increase was obtained at a porosity of ZGB-2. Folorunso and Owoeye studied that the effect of SiC content on the physical, mechanical properties and tribological behavior of stir cast ZA27 alloy based hybrid composites. They

reported that the density of the composites decreased with an increase in the SiC content while slight voids exist as compared to the unreinforced alloy [25]. The results of Brinell-hardness measurements of all composites are shown in Table 3. It can be concluded that there was a dramatic decrease in hardness values. The decrease in the $B_4C$ content resulted in higher hardness values for the hybrid nanocomposite. The results showed that $B_4C$ content harmed on the porosity of hybrid nanocomposites during hot pressing. Moreover, ZGB-2 hybrid nanocomposite contains a high proportion of Graphene and $B_4C$ supplements, the ZA27 matrix powders produced more plastic deformation and increased stresses between the matrix and the reinforcement. Yalçın et al. [9] achieved the best tribological properties in 3wt% graphene-reinforced ZA27 composites produced under similar conditions. They found the optimum performance at the composite mixture of ZA27 / 3 wt% Graphene porosity 4.05% with a Brinell hardness value of 62.67 HB.

**Table 3** The porosities and hardness value of ZA27 alloy and composites

| Sample Number | Porosity content (%) | Relative Density (%) | Brinell Hardness (HB) |
|---|---|---|---|
| ZA27 | 0.36 | 89.9 | 120 |
| ZGB-0.25 | 10.02 | 88.1 | 71.9 |
| ZGB-0.5 | 11.89 | 87.6 | 70.1 |
| ZGB-1 | 12.34 | 87.2 | 68.9 |
| ZGB-2 | 12.7 | 86.6 | 60.3 |

**Wear Mechanism**

For a better understanding of wear properties of ZA27/Graphene/$B_4C$ hybrid nanocomposites, the $B_4C$ content, and reinforcement distribution into the ZA27 matrix as well as bonding and interface interactions between ZA27/Graphene or $B_4C$ reinforcement alloys should be further investigated. For the ZA27/Graphene/$B_4C$ hybrid nanocomposites, the very critical parameter is the reinforcement content due to in the fact that microstructure changes from ZA27 alloy to hard ceramic with increasing $B_4C$ content (wt.%). The capability of burden holding increases with an increase in $B_4C$ content although the bonding strength between the ZA27 alloy and reinforcement materials decreases conspicuously. The result of the $B_4C$ content on the wear loss of the ZA27 and hybrid nanocomposites are given in Table 4. As the $B_4C$ content increased from 0.25 to 2 wt%, the wear weight loss decreased. A decrease in wear loss with increasing $B_4C$ content was observed. Between the samples codded as ZGB-1 and ZGB-2 demonstrated lower wear loss at each load when compared with the ZA27 matrix alloy. This can be attributed to the presence of graphene nanoparticles in the matrix released to wear track of the disc during performing the wear tests. Fig. 5 shows both the lubrication of graphene and the hard nanoparticle property of the $B_4C$ supplement showed a significant reduction in weight losses. Furthermore, it was shown that the relation between wear resistance and hardness is nearly linear in very advanced alloys. Girish et al. investigated the effect of graphite particles on mechanical, wear, and thermal behavior of ZA27 alloy composites. According to their results, the addition of graphite particles to the ZA27 zinc alloy matrix improves the wear resistance of the composite, the benefit of reinforcement is found more at 4–6% compared to higher values. It should be noted that a good indication that the graphite reinforcement will certainly help the designers to develop a suitable bearing material which gives better performance at elevated temperatures. However, hardness, thermal properties of composite such as thermal conductivity, diffusivity, and mechanical damping values at higher temperatures reduces with an increase in reinforcing percentage [10].

**Table 4.** The effect load on the wear loss of ZA27 alloy and hybrid nanocomposites at constant sliding distance (300m) and sliding speed (100 rpm)

| Sample | Weight loss on 1N Load (mg.) | Weight loss on 2N Load (mg.) | Weight loss on 5N Load (mg.) | Weight loss on 10N Load (mg.) |
|---|---|---|---|---|
| ZA27 | 0.36 | 1.4 | 76.6 | 250 |
| ZGB-0.25 | 0.002 | 0.003 | 0.006 | 0.028 |
| ZGB-0.5 | 0.0014 | 0.0028 | 0.005 | 0.023 |
| ZGB-1 | 0.0013 | 0.0025 | 0.004 | 0.021 |
| ZGB-2 | 0.0012 | 0.0023 | 0.0032 | 0.009 |

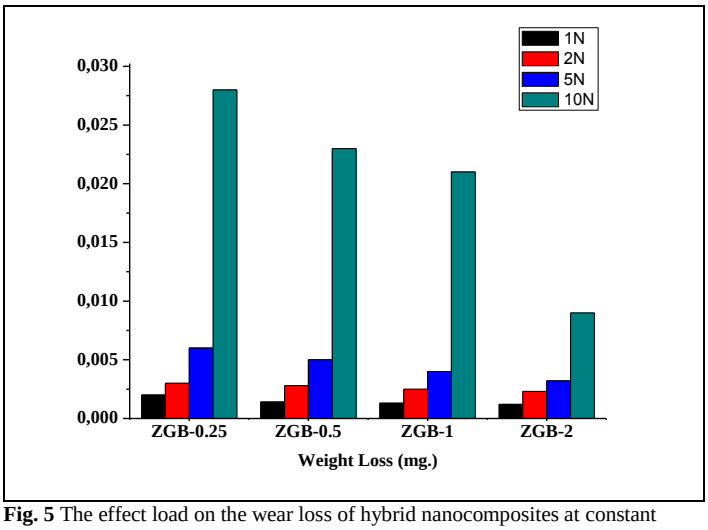


**Fig. 5** The effect load on the wear loss of hybrid nanocomposites at constant sliding distance (300 m) and sliding speed (100 rpm)

**Investigation of wear surfaces**

Fig. 6 shows the SEM views of the worn surfaces of the ZA27 matrix alloy and hybrid nanocomposites. As seen in Figure 6, the wear mechanism includes the adhesion and delimitation mechanisms. SEM analysis of the worn surfaces shows that less damaged areas were obtained after wear testing on the ZGB-2 sample (Figure 6e) compared to that of the other hybrid nanocomposites and ZA27 alloys. The increasing agglomeration can be explained by the increased $B_4C$ nanoparticle ratio. Wear marks were found on all wear surfaces in the same direction as the wear direction. In high magnifications, strips, plastic deformations, and cracks on wear surfaces were observed. As can be seen in Figure 6d-e, layer and cold tears are more common. This is because, in the experiments carried out at low loads, the particles that are detached from the sample surface have partially adhered to the surface of the sample during the test. As shown in Fig. 6, the tribological mechanism contains the abrasion and adhesion wear. The adhesion and abrasion wear that are essential tribological mechanisms describe fretting, pitting, spalling, scuffing, scoring, abrasion, and others. The increase in the $B_4C$ particle content from 0.5 to 1 results in a change of adhesion wear mechanism to abrasion. This can be attributed to the distribution of $B_4C$ particles in the ZA27 matrix. As seen in Fig. 6.b and c, even more particles have been severed, the more often the particles are bonded to the surface and the cold source has occurred. Hard $B_4C$ particles eliminate the softening of the graphene particles in the structure. Kumar stated that the microstructure of wear surfaces of ZA27-graphite composites show deep and coarse grooves on the worn surface. The addition of SiC nanoparticles and Gr particles into the alloy increased the hardness of the ZA27 matrix alloy. Also, the SiC nanoparticles hinder the plowing during wear. The grooves became shallower as the content of graphite particles was present in the ZA27 hybrid composite [26].

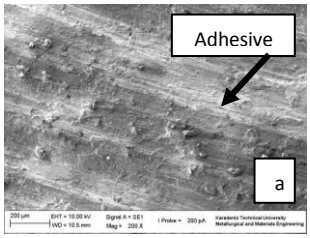


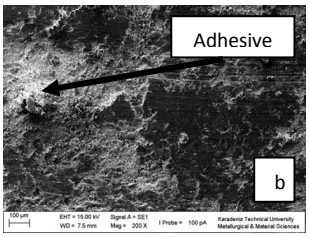

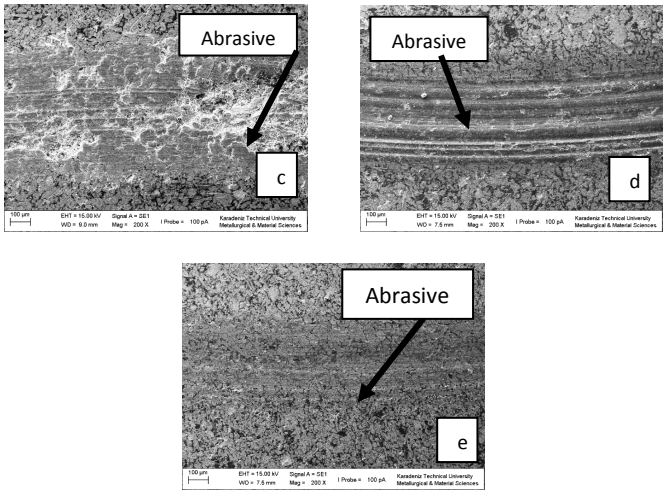


**Fig. 6** SEM images of worn surface of a) ZA27, b) ZGB-0.25, c) ZGB-0.5, d)ZGB-1 and e) ZGB-2 ball milled for 1 h

**Corrosion**

Fig. 7 shows the potentiodynamic polarization curves of ZA27 matrix alloy and ZA27 / Graphene / $B_4C$ hybrid nanocomposites ($E_{kor}$). The current density ($I_{kor}$) values decreased by the increase in $B_4C$ contents. $E_{kor}$ and low $I_{kor}$ values close to the positive indicated that the corrosion resistance of the hybrid nano composite was higher.

**Table 5** Electrochemical parameters derived from polarization data

| Sample | $I_{corr}$ ($A/cm^2$) | $E_{corr}$ (mV) | Corrosion rate (mpy) |
|---|---|---|---|
| ZA27 | 1.23 | -1000 | 2.719 |
| ZGB-0.25 | 41.7 | -1070 | 59.02 |
| ZGB-0.5 | 19.4 | -1150 | 57.6 |
| ZGB-1 | 7.5 | -968 | 20.8 |
| ZGB-2 | 16.9 | -1200 | 16.77 |

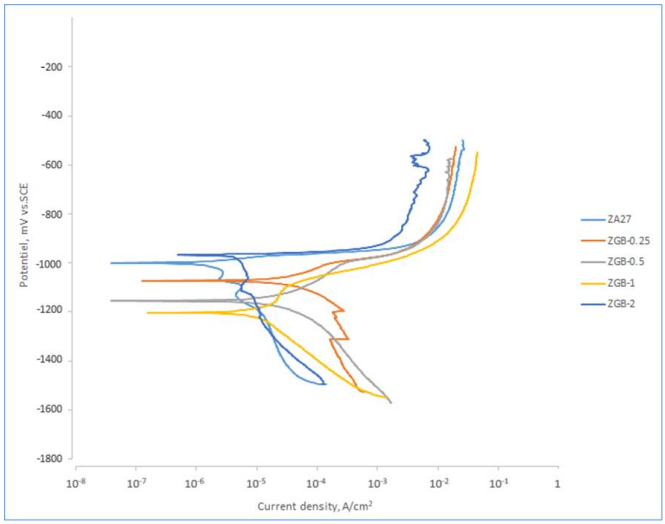


**Fig. 7** Potentiodynamic polarization curves of ZA27 alloy and hybrid nanocomposites

The polarization curves of hybrid nanocomposites showed an increase in the current density with the increase in the applied polarization. The corrosion resistance of ZGB-2 hybrid nanocomposite in the environment was higher than other hybrid nanocomposites. In determining corrosion behavior, the particle content and the passive and active state of the environment were also important. Since ceramic particle causes a reduction in corrosion resistance in an active environment, it increases the corrosion resistance in a passive environment. Also, composites with low $B_4C$ content with a $E_{kor}$ value more than others were more passive. So, the tendency to ionization was higher. The other composites are known to corrode more quickly when activated [27]. Hybrid nanocomposites have high corrosion rates. This may be due to galvanic corrosion.

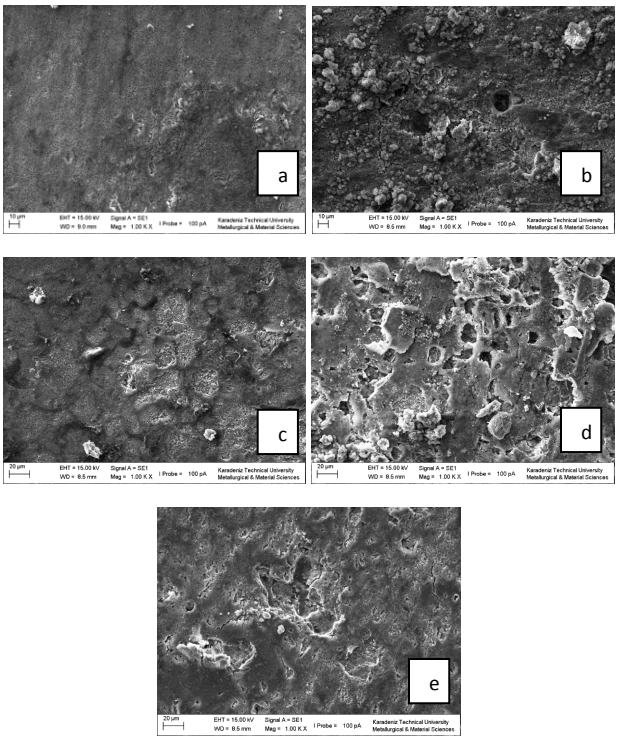


**Fig. 8** SEM images after corrosion a) ZA27, b) ZGB-0.25, c) ZGB-0.5, d) ZGB-1 and e) ZGB-2 ball milled for 1 h

Fig. 8 shows the post-corrosion SEM images of ZA27 alloy and hybrid nanocomposites. On the surface of the hybrid nanocomposite specimens, the damages were formed in different sizes after corrosion and therefore the corrosion on the surfaces of the samples was observed. This type of corrosion usually occurs in neutral environments containing chlorine. The corrosion is known to occur in passivated materials in environments involving perchlorate, iodide, bromide or chloride ions when the electrode potential passing over a critical value. The potential varies depending on the material and the corrosive structure.

**CONCLUSION**

In the current work ZA27- Graphene-$B_4C$ hybrid nanocomposites with 3wt% nano-size graphene, and 0.25 wt.%, 0.5 wt.%, 1 wt% and 2 wt.% nano-size $B_4C$ were efficiently fabricated by the hot pressing method. According to this:

1. Hybrid nanocomposites that have excellent wear resistance than the ZA27 alloy have been manufactured with supplementations graphene and $B_4C$ nanoparticles to ZA27 alloy.
2. According to SEM-EDS element distribution and XRD results of hybrid nanocomposites; Al, Zn, $CuZn_5$, $B_4C$ and Graphene phases were encountered. The amount of Al, Zn, $CuZn_5$ phases increased with an increasing amount of reinforcement.

3. Higher porosity ratio such as 2 wt.% $B_4C$ was obtained at ZGB-2 hybrid nanocomposite via hot sintering process.
4. ZGB-2 sample showed the best abrasion resistance without making grooves on the surface. Other samples exhibited an abrasive and adhesive wear mechanism. Therefore 3 wt. % nano graphene and 2 wt. % of $B_4C$ supplementation can be an excellent choice.
5. The wear resistance of hybrid nanocomposites increased with the increase in the quantity of $B_4C$ nano-sized particles.
6. The best corrosion resistance was obtained at ZGB-2 hybrid nanocomposites
7. Hybrid nanocomposites have high corrosion rates which are probably due to galvanic corrosion.

**REFERENCES**


1. Y.H. Zhu, H.C. Man and W.B. Lee: Microstructure of laser melted Zn–Al-based alloy, Journal of materials processing technology, 139, 2003, 296-301, https://doi.org/10.1016/S0924-0136(03)00239-5
2. T. Savaskan and A.P. Hekimoglu: Microstructure and mechanical properties of Zn–15Al-based ternary and quaternary alloys, Materials Science and Engineering: A, 603, 2014, 52-57, https://doi.org/10.1016/j.msea.2014.02.047
3. D. O. Folorunso and S. Owoeye: Influence of quarry dust-silicon carbide weight percentage on the mechanical properties and tribological behavior of stir cast ZA-27 alloy based hybrid composites, Journal of King Saud University - Engineering Sciences, 31(3), 2019, 280-285, https://doi.org/10.1016/j.jksues.2017.07.003
4. H. Şevik: The effect of silver on wear behaviour of zinc–aluminium-based ZA-12 alloy produced by gravity casting, Materials Characterization, 89, 2014, 81-87, https://doi.org/10.1016/j.matchar.2013.12.015
5. M. Afizadeh, M.H. Paydar and F.S. Jazi: Structural evaluation and mechanical properties of nanostructured Al/$B_4C$ composite fabricated by ARB process, Composites Part B: Engineering, 44 (1), 2013, 339-343, https://doi.org/10.1016/j.compositesb.2012.04.069
6. T. Huang, Y. Xin, T. Li, S. Nutt, C. Su, H. Chen, P. Liu and Z. Lai: Modified graphene/polyimide nanocomposites: reinforcing and tribological effects, ACS Applied Materials Interfaces, 5(11), 2013, 4878-4891, https://doi.org/10.1021/am400635x
7. A. Klemenz, L. Pastewka, S.G. Balakrishna, A. Caron, R. Bennewitz and M. Moseler: Atomic scale mechanisms of friction reduction and wear protection by graphene, Nano Letters, 12, 2014, 7145-7152, https://doi.org/10.1021/nl5037403
8. H. Aahamed and V. Senthilkumar: Consolidation behavior of mechanically alloyed aluminium based nanocomposites reinforced with nanoscale $Y_2O_3$/$Al_2O_3$ particles, Materials Characterization, 62(12), 2011, 1235-1249, https://doi.org/10.1016/j.matchar.2011.10.011
9. E. D. Yalcin, A. Canakci, F. Erdemir, H. Cuvalci and A.H. Karabacak: Enhancement of wear and corrosion resistance of ZA27/Nanographene Composites Produced by Powder Metallurgy, Arabian Journal for Science and Engineering, 7, 2018, 1437-1445, https://doi.org/10.1007/s13369-018-3582-7
10. B.M. Girish, K.R. Prakash, B.M. Satisha, P.K. Jainb, K. Devic: Need for optimization of graphite particle reinforcement in ZA27 alloy composites for tribological applications, Materials Science and Engineering A, 530, 2011, 382, https://doi.org/10.1016/j.msea.2011.09.100
11. S. Mitrovic, M. Babic and N. Miloradovic: Wear Characteristics of Hybrid Composites Based on Za27 Alloy Reinforced With Silicon Carbide and Graphite Particles, Tribology in Industry, 36(2), 2014, 204.
12. R. Dalmiş, H. Cuvalci, A. Canakci and O. Güler: Investigation of Graphite Nano Particle Addition on the Physical and Mechanical Properties of ZA27 Composite, Advanced Composites Letters, 25(2), 2016, 37-42, https://doi.org/10.1177/096369351602500202
13. Y. Dou, Y. Liu, Y. Liu, Z. Xiong and Q. Xia: Friction and wear behaviors of $B_4C$/6061Al composite, Materials & Design, 60, 2014, 669-677, https://doi.org/10.1016/j.matdes.2014.04.016
14. K. Rajkumar and S. Aravindan: Microwave sintering of copper–graphite composites, Journal of Materials Processing Technology, 209(15-16), 2009, 5601-5605, https://doi.org/10.1016/j.jmatprotec.2009.05.017
15. K.H.W. Seah, F.S.C. Sharmas and B.M. Girishs: Corrosion characteristics of ZA-27-graphite particulate composites Corrosion Science, 39(1), 1997, 1-7, https://doi.org/10.1016/S0010-938X(96)00063-7
16. B. Bobic, J. Bajat, I. Bobic, and B. Jegdic: Corrosion Influence on Surface Appearance and Microstructure of Compo Cast ZA27/SiCp Composites in Sodium Chloride Solution, Transactions of Nonferrous Metals Society of China, 26, 2016, 1512, https://doi.org/10.1016/S1003-6326(16)64257-7
17. B. O. Fatile, B. O. Adewuyi and H. T. Owoyemi: Synthesis and characterization of ZA-27 alloy matrix composites reinforced with zinc oxide nanoparticles, Engineering Science and Technology, an International Journal, 20(3), 2017, 1147-1154, https://doi.org/10.1016/j.jestch.2017.01.001
18. C. He, B. Luo, Y. Zheng, Y. Yin, Z. Bai and Z. Ren: Effect of Sn on microstructure and corrosion behaviors of Al-Mg-Si alloys, Materials, 12(13), 2019, 2069, https://doi.org/10.3390/ma12132069
19. H. Wang, X. Zhang, Z. Xu, H. Wang and C. Zhu: Hot corrosion behaviour of Al-Si coating in mixed sulphate at 1150˚C, Corrosion Science, 147, 2019, 313-320, https://doi.org/10.1016/j.corsci.2018.11.026
20. T.J. Chen, Y. Hao, Y.D. Li and Y. Ma: Effect of solid solution treatment on semisolid microstructure of dendritic zinc alloy ZA27, Materials Science and Technology, 24, 2008, 1313-1320, https://doi.org/10.1179/174328407X226716
21. Y. Liu, H.Y. Li, H. Jiang and X. Lu: Effects of heat treatment on microstructure and mechanical properties of ZA27 alloy, Transactions of Nonferrous Metals Society of China, 23(3), 2013, 642-649, https://doi.org/10.1016/S1003-6326(13)62511-X
22. Yong Xiao, Mingyu Li, Ling Wang, Shangyu Huang, Xueming Du, Zhiquan Liu, Interfacial reaction behavior and mechanical properties of ultrasonically brazed Cu/Zn–Al/Cu joints, Materials and Design 73 (2015) 42-49, https://doi.org/10.1016/j.matdes.2015.02.016
23. Dafan Du, Guang Guan, Annie Gagnoud, Yves Fautrelle, Zhongming Ren, Xionggang Lu, Hui Wang, Yinming Dai, Qiuliang Wang, Xi Li, Materials Characterization,111 (2016) 31-42, https://doi.org/10.1016/j.matchar.2015.11.004
24. Onur Güler, Fatih Erdemir, Müslim Çelebi, Hamdullah Çuvalcı, Aykut Çanakçı, Effect of nano alumina content on corrosion behavior and microstructure of Za27/graphite/alumina hybrid nanocomposites, Results in Physics 15 (2019), https://doi.org/10.1016/j.rinp.2019.102700
25. Davies Oladayo Folorunso, Seun Samuel Owoeye, Influence of quarry dust-silicon carbide weight percentage on themechanical properties and tribological behavior of stir cast ZA-27 alloybased hybrid composites, Journal of King Saud University – Engineering Sciences, 31 (2019) 280-285. https://doi.org/10.1016/j.jksues.2017.07.003
26. Nagavelly Shiva Kumar, Mechanical and Wear Behavior of ZA-27/Sic/Gr Hybrid Metal Matrix Composites, Materials Today: Proceedings 5 (2018) 19969–19975. https://doi.org/10.1016/j.matpr.2018.06.363
27. S. Gollapudi: Grain size distribution effects on the corrosion behaviour of materials, Corrosion Science, 62, 2012, 90-94, https://doi.org/10.1016/j.corsci.2012.04.040